The EMBO Journal Vol. 20 No. 7 pp. 1519–1529, 2001

The hairpin structure of the ^{6}F1^{1}F2^{2}F2 fragment from human fibronectin enhances gelatin binding

Andrew R.Pickford, Steven P.Smith, David Staunton, Jonathan Boyd and Iain D.Campbell[1]

Department of Biochemistry and Oxford Centre for Molecular Sciences, University of Oxford, South Parks Road, Oxford OX1 3QU, UK

[1]Corresponding author
e-mail: idc@bioch.ox.ac.uk

The solution structure of the ^{6}F1^{1}F2^{2}F2 fragment from the gelatin-binding region of fibronectin has been determined (Protein Data Bank entry codes 1e88 and 1e8b). The structure reveals an extensive hydrophobic interface between the non-contiguous ^{6}F1 and ^{2}F2 modules. The buried surface area between ^{6}F1 and ^{2}F2 (~870 Å^{2}) is the largest intermodule interface seen in fibronectin to date. The dissection of ^{6}F1^{1}F2^{2}F2 into the ^{6}F1^{1}F2 pair and ^{2}F2 results in near-complete loss of gelatin-binding activity. The hairpin topology of ^{6}F1^{1}F2^{2}F2 may facilitate intramolecular contact between the matrix assembly regions flanking the gelatin-binding domain. This is the first high-resolution study to reveal a compact, globular arrangement of modules in fibronectin. This arrangement is not consistent with the view that fibronectin is simply a linear 'string of beads'.

Keywords: assembly/collagen/dissection/extracellular matrix/fibronectin

Introduction

The extracellular matrix glycoprotein fibronectin is a large, multifunctional molecule involved in adhesion and migration events in a range of important physiological processes such as embryogenesis, wound healing, haemostasis and thrombosis (Hynes, 1990). As a soluble dimer in plasma, it is involved in blood coagulation through its affinity for fibrin and platelets. As an insoluble network in the extracellular matrix, it interacts with cell surface receptors and with other matrix components such as collagens and proteoglycans, thus assisting cell migration and the maintenance of tissue integrity (Hynes, 1990).

The interaction between fibronectin and collagen in the extracellular matrix is well documented (Hynes, 1990) but poorly understood at the molecular level. The two proteins are co-distributed in tissues, as shown by immunofluorescence and immunocytochemical studies. Addition of extraneous fibronectin also promotes the attachment of fibroblastic cells to collagen substrates *in vitro*. Furthermore, fibronectin is observed in a regularly distributed array along collagen fibres synthesized in culture. Knowledge of the molecular basis of fibronectin's interaction with collagen would provide a better understanding of the structure and function of the extracellular matrix.

The only viable approach to correlating the structure and function of the large, flexible fibronectin monomer at the atomic level is to dissect it into manageable units (Campbell and Downing, 1998). Fortunately, like many other proteins of the extracellular matrix, fibronectin is a mosaic protein consisting of repeating sequence elements or 'modules' that are capable of folding independently (Bork *et al*., 1996). Its primary sequence is composed almost entirely of three types of module (F1, F2 and F3), which are organized into functional domains (Figure 1A). These domains may be isolated in the form of proteolytic fragments that retain affinity for various ligands. Consequently, many of the ligand-binding sites have been mapped to specific regions of the fibronectin polypeptide. The collagen-binding domain can be isolated as a 42 kDa proteolytic fragment that retains affinity for heat-denatured collagen (gelatin) (Hynes, 1990). This domain has the module composition ^{6}F1^{1}F2^{2}F2^{7}F1^{8}F1^{9}F1, where ^{n}F*X* represents the *n*th type *X* module in the native protein. Further dissection of this gelatin-binding domain by proteolysis produces three non-overlapping module pairs (^{6}F1^{1}F2, ^{2}F2^{7}F1 and ^{8}F1^{9}F1) each of which retains some degree of gelatin-binding activity (Ingham *et al*., 1989; Litvinovich *et al*., 1991). This suggests that the gelatin-binding site (or sites) spans multiple modules in the domain.

Attempts to localize the gelatin-binding site further by recombinant expression in *Escherichia coli* have yielded conflicting results. Analysis of recombinant fragments produced as β-galactosidase fusion proteins showed that both the ^{1}F2 module and the ^{1}F2^{2}F2 module pair could bind immobilized gelatin (Banyai *et al*., 1990). In an earlier study, however, the ^{6}F1^{1}F2^{2}F2 module construct only bound to gelatin if the 14 N-terminal residues of ^{7}F1 were present at the C-terminus of the triplet fragment (Owens and Baralle, 1986). A third study identified the smallest recombinant fragment capable of binding to immobilized gelatin as ^{6}F1^{1}F2^{2}F2^{7}F1 (Skorstengaard *et al*., 1994). The occurrence of F2 modules in other gelatin-binding proteins, such as the matrix metalloproteinases (MMP) 2 and 9, provides evidence for their involvement in gelatin binding by fibronectin (Collier *et al*., 1988; Wilhelm *et al*., 1989). Furthermore, recombinant expression of F2 modules from these MMPs has produced fragments with high affinity for gelatin (Banyai and Patthy, 1991; Collier *et al*., 1992; Banyai *et al*., 1994), whereas recombinant MMP2 lacking F2 modules was devoid of gelatin-binding activity (Murphy *et al*., 1994; Allan *et al*., 1995).

Here we describe the gelatin-binding properties and solution structure of the ^{6}F1^{1}F2^{2}F2 fragment from fibronectin (Protein Data Bank entry codes 1e88 and 1e8b).

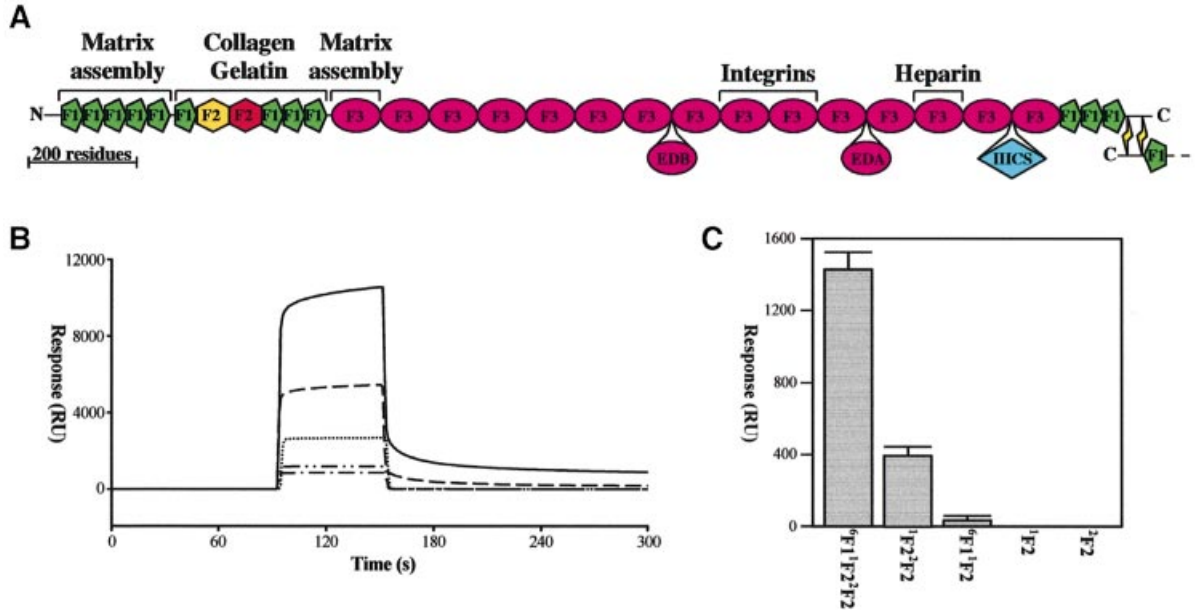

Fig. 1. Binding of fibronectin fragments to immobilized collagen α1(I) chains. (**A**) The mosaic structure of a fibronectin monomer is shown, with the positions of the alternatively spliced regions EDB, EDA and IIICS depicted below. The major binding sites for cells and for other matrix components are labelled. (**B**) Assaying the binding of fibronectin fragments to immobilized α1 chains by surface plasmon resonance (SPR). A 20 µl aliquot of 300 µM samples of $^{6}F1^{1}F2^{2}F2$ (—), $^{1}F2^{2}F2$ (– – –), $^{6}F1^{1}F2$ (.....), $^{1}F2$ (– - – -) and $^{2}F2$ (– - - –) was injected over the same flow cell of immobilized collagen α1(I) chains at a flow rate of 20 µl/min. The surface was regenerated with 50 mM HCl after each injection and the individual sensorgrams overlaid with the BIAevaluation 3.0 software (Biacore). (**C**) Response (RU) 25 s after the end of the injection of the fibronectin fragments as a comparison of collagen α1(I) chain binding ability. Significant binding was only detected in this assay for $^{6}F1^{1}F2^{2}F2$ and $^{1}F2^{2}F2$. Values represent the mean of triplicate samples, with standard deviation of replicate samples shown as error bars.

Dissection of this fragment into the $^{6}F1^{1}F2$ module pair and the individual $^{2}F2$ module results in a drastic reduction in gelatin affinity, suggesting that module–module interactions are essential for optimal binding activity. A comparison of backbone amide chemical shifts of $^{6}F1^{1}F2^{2}F2$ with $^{6}F1^{1}F2$ and $^{1}F2^{2}F2$ revealed long-range interactions between the non-contiguous $^{6}F1$ and $^{2}F2$ modules. In the solution structure of $^{6}F1^{1}F2^{2}F2$, the $^{6}F1$ and $^{2}F2$ modules interact via an extensive hydrophobic interface whose buried surface area is the largest intermodule contact yet seen in fibronectin. The central $^{1}F2$ module shows no non-covalent interactions with either $^{6}F1$ or $^{2}F2$, implying that the $^{6}F1$–$^{1}F2$ interface observed previously (Bocquier *et al.*, 1999) is disrupted in the presence of additional modules. The hairpin topology of $^{6}F1^{1}F2^{2}F2$ may facilitate intramolecular contact between the flanking $^{1}F1^{2}F1^{3}F1^{4}F1^{5}F1$ and $^{1}F3$ fragments, an interaction that is believed to modulate fibronectin fibrillogenesis in the extracellular matrix. Its conformation may also account for the previously noted disruptions in the otherwise uniform strand-like images seen in electron micrographs of fibronectin at high ionic strength. This is the first high-resolution study to reveal a compact, globular arrangement of modules in fibronectin.

Results and discussion

Enhanced gelatin-binding activity in the $^{6}F1^{1}F2^{2}F2$ fragment

The isolated $^{1}F2$ and $^{2}F2$ modules, the $^{6}F1^{1}F2$ and $^{1}F2^{2}F2$ module pairs and the $^{6}F1^{1}F2^{2}F2$ module triplet were produced as described in Materials and methods. During their purification, the isolated $^{1}F2$ and $^{2}F2$ modules and the $^{6}F1^{1}F2$ module pair bound weakly to the gelatin affinity column and were separated from the non-binding contaminants by isocratic elution; the $^{1}F2^{2}F2$ module pair and the $^{6}F1^{1}F2^{2}F2$ module triplet bound more tightly and were eluted with a urea gradient.

The binding of $^{1}F2$, $^{2}F2$, $^{6}F1^{1}F2$, $^{1}F2^{2}F2$ and $^{6}F1^{1}F2^{2}F2$ to immobilized collagen α1(I) chains was analysed in greater detail using surface plasmon resonance (SPR) (Figure 1B and C). For the $^{6}F1^{1}F2^{2}F2$ binding to the α1(I) polypeptide chains, an acceptable fit (χ^2 <2) could be obtained with a model that assumed surface heterogeneity, a common observation of immobilization through amine side chains. This treatment resolved the data into two components, with the major component exhibiting association (k_{on}) and dissociation (k_{off}) rates of 115 ± 12 $M^{-1}s^{-1}$ and 0.0036 ± 0.001 s^{-1}, respectively, and an equilibrium dissociation constant of 31 ± 6 µM ($K_d = k_{off}/k_{on}$). No significant changes in the $^{6}F1^{1}F2^{2}F2$ binding were observed under acidic conditions (pH 4.5). The $^{1}F2^{2}F2$ bound with much lower affinity, with k_{on} and k_{off} values of 94 ± 21 $M^{-1}s^{-1}$ and 0.012 ± 0.001 s^{-1}, respectively, which is equivalent to an equilibrium dissociation constant of 131 ± 23 µM. The binding of $^{1}F2$, $^{2}F2$ and $^{6}F1^{1}F2$ to immobilized α1(I) chains was too weak to quantify the kinetics with this assay.

The very low affinity of the $^{1}F2$ and $^{2}F2$ modules and of the $^{6}F1^{1}F2$ module pair for α1(I) chains demonstrates that the gelatin-binding site of $^{6}F1^{1}F2^{2}F2$ does not reside entirely within any single module (Figure 1C). The moderate affinity of the $^{1}F2^{2}F2$ module pair may result from cooperativity between weak, independent binding

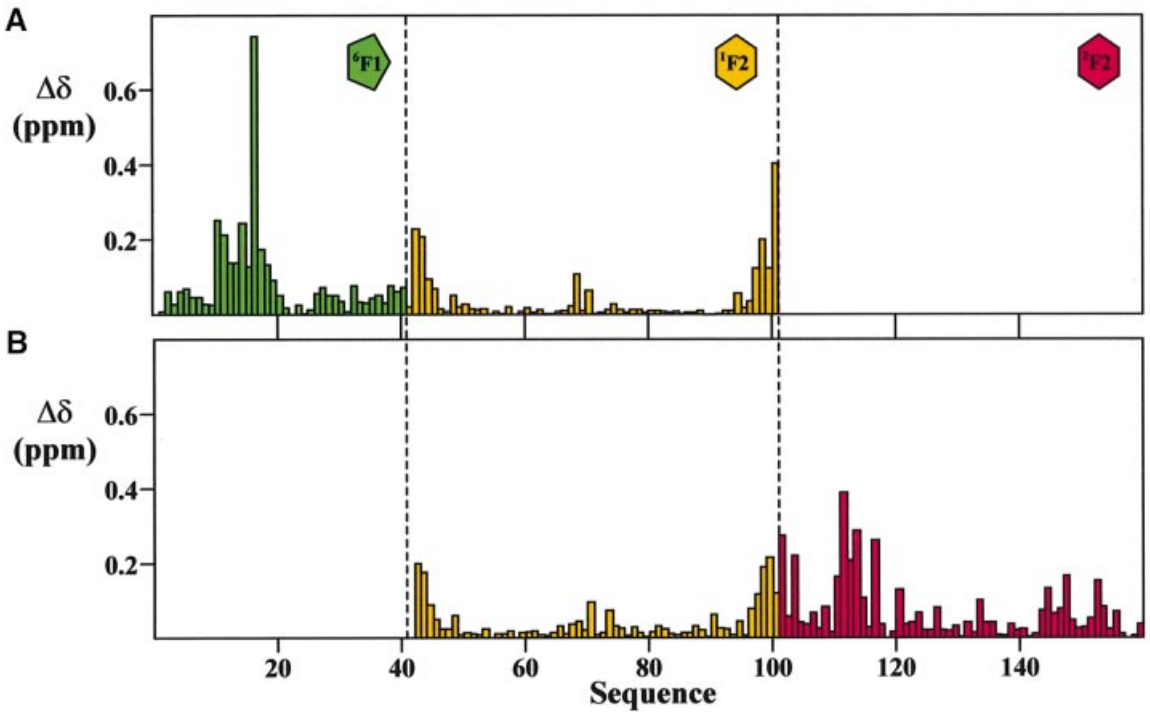

Fig. 2. Amide chemical shift perturbation upon dissection of $^{6}F1^{1}F2^{2}F2$. (A and B) Combined chemical shift perturbation (Δδ) of the H^{N} and N^{H} backbone resonances, upon (**A**) removal of the $^{2}F2$ module from $^{6}F1^{1}F2^{2}F2$, and (**B**) removal of the $^{6}F1$ module from $^{6}F1^{1}F2^{2}F2$. In each case, $\Delta\delta = \{|\Delta\delta H^{N}| + (|\Delta\delta N^{H}|/5)\}/2$, where $\Delta\delta H^{N}$ and $\Delta\delta N^{H}$ are the amide proton and amide nitrogen chemical shift differences, respectively.

sites on each module since there is no defined interface between the modules and they tumble independently of each other (Smith *et al*., 2000). The enhanced binding activity of $^{6}F1^{1}F2^{2}F2$ must therefore involve the formation of a composite binding site involving $^{1}F2$ and/or $^{2}F2$ and the $^{6}F1$ module, or cooperativity between independent, weak gelatin-binding sites on separate modules. The structural basis for this affinity was investigated by nuclear magnetic resonance (NMR) spectroscopy.

$^{6}F1$ and $^{2}F2$ interact in the $^{6}F1^{1}F2^{2}F2$ fragment

Preliminary information regarding the nature and site of any intermodule interaction in a mosaic protein can be derived from a comparison of the NMR chemical shifts of overlapping fragments under identical solution conditions. We compared the backbone amide resonances (N^{H} and H^{N}) of the $^{6}F1^{1}F2^{2}F2$ fragment with the overlapping $^{6}F1^{1}F2$ and $^{1}F2^{2}F2$ module pairs (Figure 2). Removal of the $^{2}F2$ module from $^{6}F1^{1}F2^{2}F2$ results in shift perturbations at the C-terminus of the $^{1}F2$ module (Figure 2A), as expected from the change in charge. However, many major shift changes are seen in $^{6}F1$, in the region of Val10–Lys20. Similarly, removal of $^{6}F1$ from $^{6}F1^{1}F2^{2}F2$ results in shift perturbations at the N-terminus of the $^{1}F2$ module, but the largest shift changes are seen in the $^{2}F2$ module, in the region of Ser111–His117 (Figure 2B). Therefore, the $^{6}F1$ and $^{2}F2$ modules must interact in $^{6}F1^{1}F2^{2}F2$ despite being separated in sequence by the $^{1}F2$ module.

Solution structure of $^{6}F1^{1}F2^{2}F2$

The solution structure of the $^{6}F1^{1}F2^{2}F2$ fragment could, in theory, be modelled by combining the NMR restraints derived from the independent studies on the overlapping $^{6}F1^{1}F2$ and $^{1}F2^{2}F2$ module pairs (Bocquier *et al*., 1999; Smith *et al*., 2000). However, because of the extensive amide chemical shift changes in the $^{6}F1$ and $^{2}F2$ modules, and thus the possibility of significant structural alterations, the solution structure was determined *ab initio* using only restraints derived from NMR experiments on $^{6}F1^{1}F2^{2}F2$ itself. Of the 100 structures calculated, 20 were selected on the basis of their good agreement with the experimental restraints and their minimal deviations from ideal covalent geometry (Table I).

The tertiary structures of the individual modules in $^{6}F1^{1}F2^{2}F2$ are very similar to those in previous studies of the $^{6}F1^{1}F2$ module pair (Bocquier *et al*., 1999) and the isolated $^{2}F2$ module (Sticht *et al*., 1998). The backbone heavy atom (N^{H}, Cα, C) root mean square (r.m.s.) deviations over secondary structure elements are 0.98 Å for $^{6}F1$, 0.65 Å for $^{1}F2$ and 1.21 Å for $^{2}F2$. The $^{6}F1$ module (Figure 3A) comprises a short N-terminal double-stranded antiparallel β-sheet (*AB*) that folds over a triple-stranded β-sheet (*CDE*). The β-sheets are linked by two, conserved disulfide bridges in a 1–3 and 2–4 pattern connecting strands *A–D* and *D–E*, respectively. The module core is composed primarily of two highly conserved aromatic residues Tyr12 and Trp18, and a hydrophobic residue, Val36.

The $^{1}F2$ module (Figure 3B) comprises two double-stranded antiparallel β-sheets (*AB* and *CD*), oriented approximately perpendicular to each other, with a single α-helical turn located between strands *C* and *D*. The cleft between the β-sheets is occupied by side chains of invariant hydrophobic and aromatic residues, which make up the module core. On the opposite face of the

Table I. Experimental restraints and structural statistics

R.m.s. deviations from experimental data[a]	
all 2024 NOE restraints	0.009 ± 0.001 Å
515 intraresidue NOEs {$i = j$}	0.008 ± 0.002 Å
598 sequential NOEs {$\|i–j\| = 1$}	0.007 ± 0.002 Å
231 short-range NOEs {$1 < \|i–j\| < 5$}	0.014 ± 0.003 Å
539 long-range NOEs {$\|i–j\| > 4$}	0.009 ± 0.002 Å
41 ^{6}F1–^{2}F2 intermodule NOEs	0.006 ± 0.003 Å
100 ambiguous NOEs	0.011 ± 0.004 Å
106 hydrogen bond restraints	0.010 ± 0.002 Å
69 dihedral φ angles	0.066 ± 0.036°
R.m.s. deviations from ideal covalent geometry	
bonds	0.0013 ± 0.0001 Å
angles	0.245 ± 0.004°
impropers	0.123 ± 0.014°
Ramachandran analysis[b]	
residues in favoured regions	55.0%
residues in additional allowed regions	39.9%
residues in generously allowed regions	4.4%
residues in disallowed regions	0.7%
Coordinate precision: secondary structure backbone, all heavy atoms[c]	
^{6}F1(^{1}F2^{2}F2)	0.46 ± 0.17 Å, 1.21 ± 0.82 Å
(^{6}F1)^{1}F2(^{2}F2)	0.33 ± 0.09 Å, 0.99 ± 0.88 Å
(^{6}F1^{1}F2)^{2}F2	0.37 ± 0.06 Å, 0.98 ± 0.69 Å
^{6}F1(^{1}F2)^{2}F2	0.53 ± 0.14 Å, 1.15 ± 0.73 Å
(^{6}F1)^{1}F2(^{2}F2)	11.7 ± 3.48 Å, 10.2 ± 3.59 Å

[a]None of the 20 accepted structures showed distance restraint violations of >0.3 Å or dihedral restraint violations of >2°. No distance or dihedral restraints were consistently violated by >0.1 Å or 1°, respectively.
[b]Prolines, glycines and terminal residues are excluded.
[c]Coordinate r.m.s. deviations were calculated following best-fit superposition over the secondary structure elements of the underlined module(s). Residues from modules in parentheses were excluded from the calculation.

second β-sheet, two disulfide bonds link the invariant cysteines, with connectivities 1–3 and 2–4. The topology of ^{2}F2 (Figure 3C) is very similar to that of ^{1}F2, but includes the additional *A′A″* β-sheet preceding the first cysteine residue.

In general, the individual ^{6}F1, ^{1}F2 and ^{2}F2 modules in ^{6}F1^{1}F2^{2}F2 are well defined (Figure 3A–C) with low backbone heavy atom r.m.s. deviations over their secondary structure elements (Table I). The low ^{15}N-{^{1}H}-NOE for the *C–D* loop in ^{6}F1, and the *B–C* loops in ^{1}F2 and ^{2}F2, each of which have backbone r.m.s. deviations >1.0 Å, shows that the poorer definition of these regions arises from backbone flexibility rather than a lack of experimental data (Figure 3D and E).

The list of long-range NOEs used in the final round of ^{6}F1^{1}F2^{2}F2 structure calculations included an extensive array of intermodule restraints between nine residues in ^{6}F1 and eight in ^{2}F2 (Table I). This resulted in a precise definition of the relative locations and orientations of the ^{6}F1 and ^{2}F2 modules in ^{6}F1^{1}F2^{2}F2 (Figure 4; Table I). The ^{6}F1–^{2}F2 interface is formed by the docking of the external edges of β-strands *C* of ^{6}F1 and *A′* of ^{2}F2, and by the annealing of two extensive hydrophobic surfaces involving Val10, Tyr12, Met16, Leu19 and Leu28 from ^{6}F1, and Leu103, Ala114, Leu115 and Thr145 from ^{2}F2 (Figure 5A). These non-polar residues account for 53% of the total buried surface area between the two modules. There are no titratable groups involved in the remaining 47% that could disrupt the hairpin topology within the pH range 4.5–7.4.

No long- or short-range NOEs were observed, either between the ^{6}F1 and ^{1}F2 modules, or between the ^{1}F2 and ^{2}F2 modules. The ^{6}F1–^{1}F2 and ^{1}F2–^{2}F2 linker sequences are flexible, as indicated by their low ^{15}N-{^{1}H}-NOE values (Figure 3E). Hence, the relative location and orientation of ^{1}F2 are somewhat ill defined (Figure 4A; Table I) since the only positional constraints on this central module are the covalent tethering of its N- and C-termini, and steric hindrance from ^{6}F1 and ^{2}F2.

The gelatin-binding site(s) of ^{6}F1^{1}F2^{2}F2

In each F2 module, five of the core aromatic residues (Tyr62, Trp81, Tyr88, Tyr94 and Phe96 in ^{1}F2; Tyr122, Trp141, Tyr148, Phe154 and Phe156 in ^{2}F2) form an extensive, solvent-exposed hydrophobic surface (Figure 3B and C). A pocket in each of these surfaces is thought to provide a binding site for non-polar residues in type I collagen (Pickford *et al*., 1997). This is supported by the binding of the collagen-like peptide (Pro-Pro-Gly)$_6$ to the ^{2}F2 module from MMP2, which produced backbone H^N and N^H chemical shift perturbations in the equivalent residues (Briknarová *et al*., 1999). Furthermore, in the crystal structure of pro-MMP2, a phenylalanine side chain in the inhibitory propeptide occupies the equivalent hydrophobic pocket in the ^{3}F2 module, preventing it from binding its gelatin substrate (Morgunova *et al*., 1999).

In all structures of the ^{6}F1^{1}F2^{2}F2 ensemble, solvent access to the putative binding sites on the F2 modules is unhindered by the ^{6}F1–^{2}F2 interface. In the average ^{6}F1^{1}F2^{2}F2 structure (Figure 5A), the binding sites are oriented in opposite directions. This configuration of F2 modules observed here is reminiscent of the pro-MMP2 crystal structure where the three F2 modules are also oriented with their binding sites facing outwards (Morgunova *et al*., 1999). Recombinant ^{1}F2^{2}F2^{3}F2 from MMP2 has been shown to be capable of binding multiple collagen triple helices (Steffensen *et al*., 1995), suggesting that F2 modules form separate binding surfaces that intercalate between molecules in a collagen fibril. The flexibility of the ^{1}F2 module with respect to ^{6}F1 and ^{2}F2 may permit a variety of collagen-binding conformations. It has also been proposed that the observed pliability of the ^{9}F3^{10}F3 module pair may allow it to accommodate some variation in the integrin structure to which it binds (Copié *et al*., 1998).

The structural basis for the 4-fold increase in affinity for α(I) chains from ^{1}F2^{2}F2 to ^{6}F1^{1}F2^{2}F2 is not known, but may arise from an extension of the ^{2}F2 binding site onto ^{6}F1. The ^{6}F1 module docks onto ^{2}F2 alongside its gelatin-binding site in an orientation that may allow solvent-exposed residues in the *AB* sheet of ^{6}F1 to contribute to binding (Figure 4B). Alternatively, the binding enhancement may arise from stabilization of the ^{2}F2 module due to the ^{6}F1–^{2}F2 interface. The backbone H^N protons of residues within the *AB* sheet of ^{6}F1 and the *A′A″* sheet of ^{2}F2 undergo much slower solvent exchange in ^{6}F1^{1}F2^{2}F2 than observed previously for ^{6}F1^{1}F2 (Bocquier *et al*., 1999) and ^{2}F2 (Sticht *et al*.,

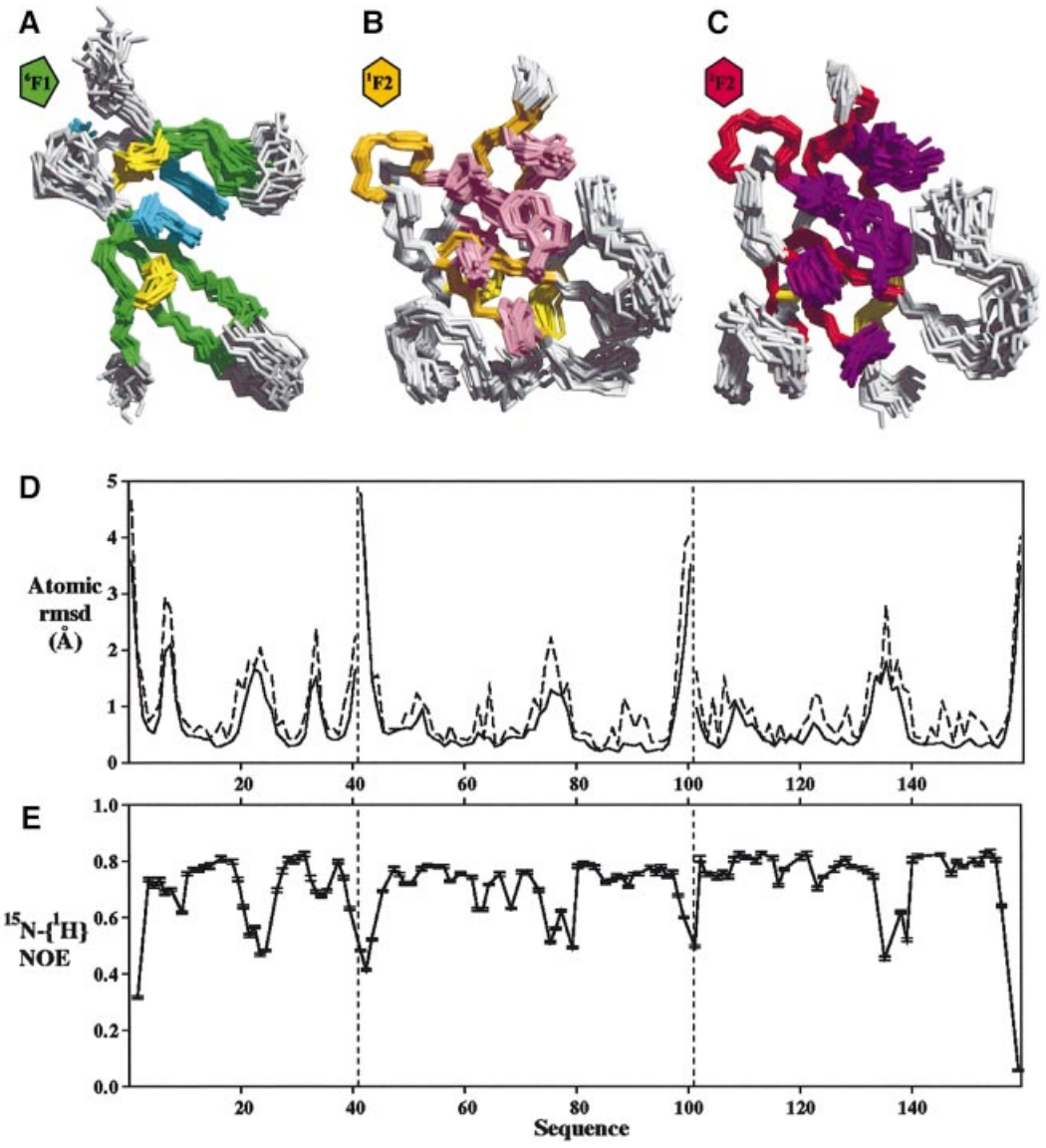

Fig. 3. Structural definition of the individual modules in ^{6}F1^{1}F2^{2}F2. (**A–C**) Individual module overlays for the ensemble of 20 lowest energy structures of ^{6}F1^{1}F2^{2}F2. Each module has been overlaid onto the lowest energy structure by best-fit superposition over the backbone heavy atoms of its secondary structure elements. The secondary structure is coloured green in ^{6}F1, gold in ^{1}F2 and red in ^{2}F2. The disulfide bridges are shown in yellow, and the side chains of non-polar residues that are invariant or highly conserved between modules are shown in cyan for ^{6}F1, pink for ^{1}F2 and purple for ^{2}F2. (**D**) Average atomic r.m.s. deviation between the 20 accepted structures for the backbone heavy atoms (solid line) and all heavy atoms (dotted line). The vertical dashed lines mark the exon boundaries between the modules. (**E**) ^{15}N-{^{1}H}-NOE for the ^{6}F1^{1}F2^{2}F2 fragment. Lower ^{15}N-{^{1}H}-NOE values indicate regions with increased backbone flexibility.

1998). Stabilization of the ^{2}F2 module was observed previously in differential scanning calorimetric studies on the ^{6}F1^{1}F2^{2}F2^{7}F1 proteolytic fragment, although this was originally attributed to an interaction between ^{1}F2 and ^{2}F2 (Litvinovich *et al*., 1991).

The contributions of ^{7}F1, ^{8}F1 and ^{9}F1 to collagen binding have yet to be determined. The only structural information available for these domains is the isolated ^{7}F1 (Baron *et al*., 1990), but there is no information on its interactions with adjacent modules. Given the hairpin structure observed in ^{6}F1^{1}F2^{2}F2, we believe that the extension of the ^{6}F1^{1}F2^{2}F2 nucleus with these modules will provide a better examination of the collagen-binding domain function.

Module reorganization upon dissection

The two techniques capable of providing high-resolution structural information on binding surfaces, namely X-ray diffraction and NMR, are both limited in the size of mosaic proteins that can be studied (Campbell and Downing, 1998). In the case of X-ray diffraction, the limitation arises from the difficulty in crystallizing a protein that is inherently flexible, whilst for NMR the molecular weight is the limiting factor. Hence, for both techniques, large mosaic proteins must frequently be dissected into fragments that are amenable to analysis. However, a comparison of the solution structures of ^{6}F1^{1}F2 and ^{6}F1^{1}F2^{2}F2 illustrates a potential complication associated with this dissection strategy (Figure 5).

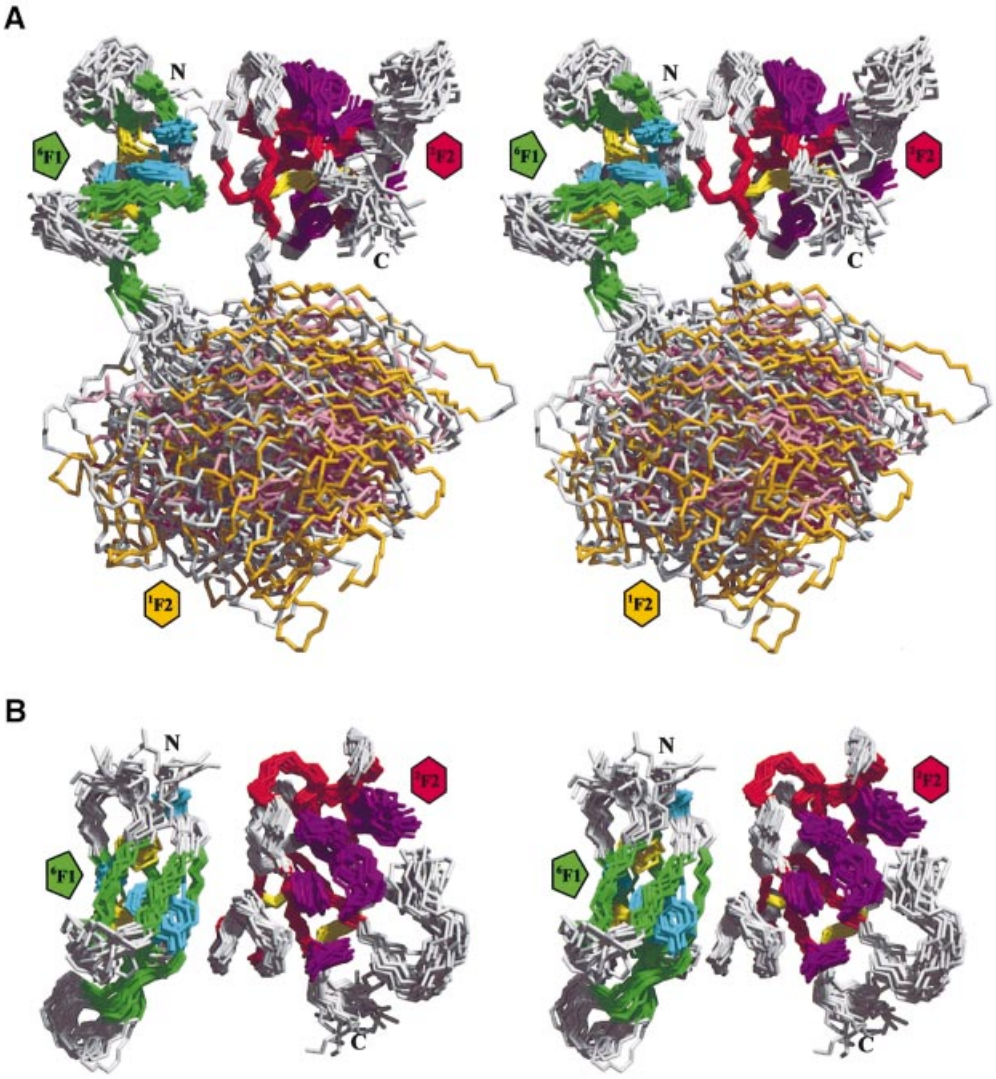

Fig. 4. Solution structure of ^{6}F1^{1}F2^{2}F2. (**A**) A stereoview of the ensemble of the 20 lowest energy structures of ^{6}F1^{1}F2^{2}F2 is shown. The structures were superimposed on the backbone heavy atoms of the secondary structure elements of the ^{6}F1 and ^{2}F2 modules of the lowest energy structure. The colour scheme for the protein backbone and side chain residues is the same as in Figure 3A–C. (**B**) Orthogonal stereoview of the ^{6}F1^{1}F2^{2}F2 ensemble generated by a 90° rotation about the horizontal. For clarity, the disordered ^{1}F2 module has been omitted.

The F1 and F2 modules in ^{6}F1^{1}F2 were found to interact via a small hydrophobic interface of ~340 Å^{2}, involving the side chains of Leu19 and Leu28 from ^{6}F1, and Tyr68 from ^{1}F2 (Bocquier *et al*., 1999). This interaction resulted in a significant upfield shift in the N^{H} resonance of Ser69 relative to the isolated ^{1}F2 module (Hashimoto *et al*., 2000). However, this ^{6}F1–^{1}F2 interface is inconsistent with the solution structure of ^{6}F1^{1}F2^{2}F2 presented here. The upfield shift of the Ser69 N^{H} resonance is reversed in ^{6}F1^{1}F2^{2}F2, consistent with a break up of the weak ^{6}F1–^{1}F2 interface (Figure 2A). None of the 18 weak intermodule NOEs previously observed between ^{6}F1 and ^{1}F2 is apparent in the spectra of ^{6}F1^{1}F2^{2}F2; manual incorporation of these restraints into the structure calculations of ^{6}F1^{1}F2^{2}F2 also resulted in structures with 20–25% higher potential energy. Therefore, this contact between the modules must have arisen from a module reorganization; removal of the ^{2}F2 module relieves the covalent and steric constraints on the ^{1}F2 module, allowing a hydrophobic collapse of non-polar residues that are distant and/or buried in the intact protein (Figure 5). Such rearrangements are a well-known phenomenon in intracellular proteins, for example, the rearrangement of SH2 and SH3 domains in Src family tyrosine kinases (Sicheri *et al*., 1997).

A globular domain in a fibrillar protein

The ^{6}F1–^{2}F2 interface gives the ^{6}F1^{1}F2^{2}F2 fragment a compact, hairpin topology (with average dimensions 15 × 19 × 32 Å). This is in sharp contrast to the extended, near-linear arrangement of F3 modules in the crystal structures of the cell-binding ^{7}F3^{8}F3^{9}F3^{10}F3 (Leahy *et al*., 1996) and heparin-binding ^{12}F3^{13}F3^{14}F3 (Sharma *et al*., 1999) fragments of fibronectin (Figure 6). The global topology of ^{6}F1^{1}F2^{2}F2 is in agreement with previous calorimetric studies, which suggested that the gelatin-binding domain has a relatively compact structure (Litvinovich *et al*., 1991).

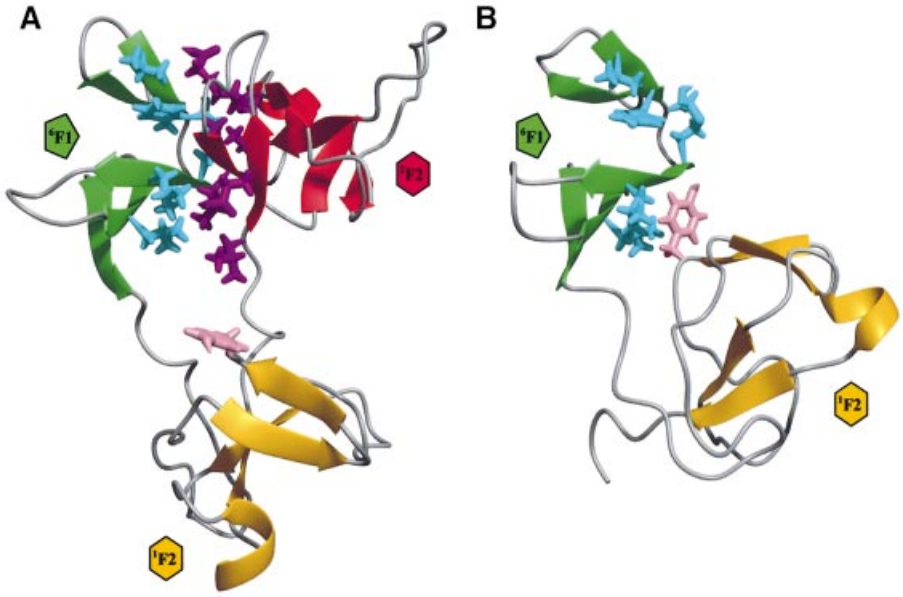

Fig. 5. Module reorganization upon dissection of $^{6}F1^{1}F2^{2}F2$. Ribbon diagrams of the minimized average structures of (**A**) $^{6}F1^{1}F2^{2}F2$ and (**B**) $^{6}F1^{1}F2$. The colour scheme for the secondary structure elements is as in Figure 3A–C. Side chains for which $^{6}F1$–$^{2}F2$ intermodule NOEs were observed (V10, Y12, S13, M16, L19 and L28 of $^{6}F1$, and L103, Q105, S111, N112, A114, L115, T145 and K153 for $^{2}F2$) are shown in cyan for $^{6}F1$ and purple for $^{2}F2$. Removal of the $^{2}F2$ module allows the side chain of Y68 (pink) in $^{1}F2$ to interact with L19 and L28 in $^{6}F1$.

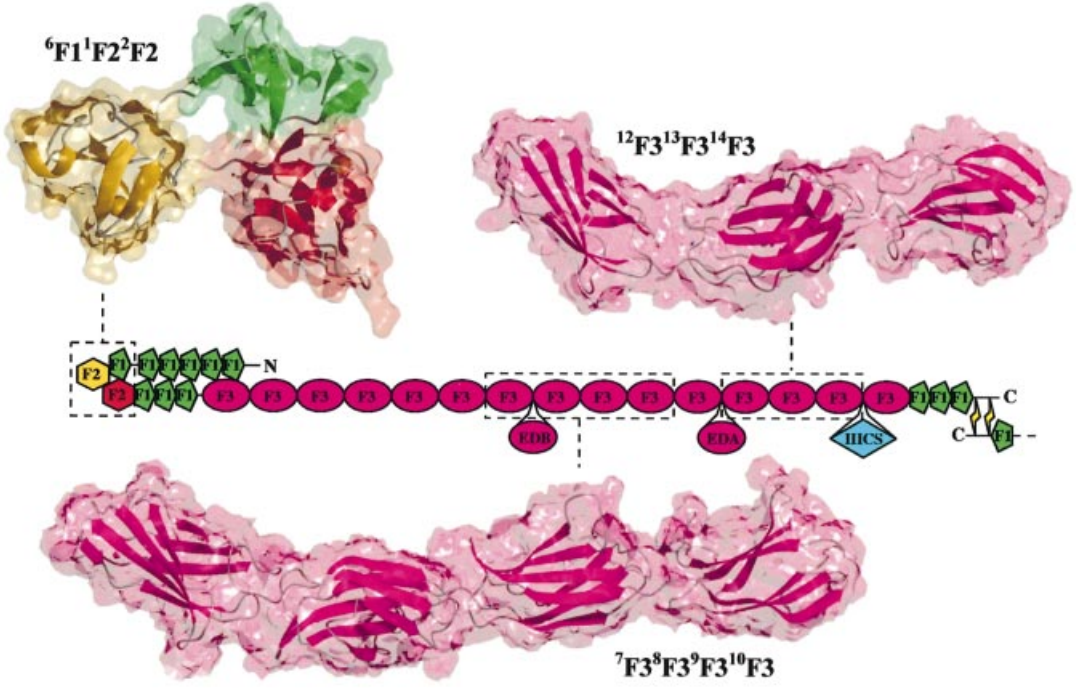

Fig. 6. Global topologies of multimodule fibronectin fragments. Solvent-accessible surfaces have been superimposed over ribbon diagrams for the minimized average structure of $^{6}F1^{1}F2^{2}F2$, and the crystal structures of $^{7}F3^{8}F3^{9}F3^{10}F3$ (Leahy *et al*., 1996) and $^{12}F3^{13}F3^{14}F3$ (Sharma *et al*., 1999). The fragment structures are mapped onto the mosaic illustration of fibronectin, which has been folded to account for the hairpin structure of $^{6}F1^{1}F2^{2}F2$.

Numerous biophysical and biochemical studies have shown that intact fibronectin undergoes a substantial change in structure from a compact conformation at low ionic strength to a more extended conformation in high salt (Engel *et al*., 1981; Erickson *et al*., 1981; Erickson and Carrell, 1983; Rocco *et al*., 1983; Lai *et al*., 1993). However, even at high ionic strength, numerous kinks are seen in electron micrographs of the molecule (Engel *et al*., 1981; Erickson *et al*., 1981; Erickson and Carrell, 1983; Rocco *et al*., 1983; Lai *et al*., 1993; Johnson *et al*., 1999). The resistance of these bends in the protein to high salt concentrations suggests that the interactions involved are predominantly non-polar in nature. Thus, the solution structure of $^{6}F1^{1}F2^{2}F2$ presented here, with its hairpin conformation and extensive hydrophobic interface between the $^{6}F1$ and $^{2}F2$ modules, is one possible

explanation for the kinks observed towards the N-terminal ends of the fibronectin dimer (Figure 6).

Many of the models for the compact structure of fibronectin at low ionic strength involve a folding over of the ^{1}F1^{2}F1^{3}F1^{4}F1^{5}F1 fragment allowing it to form interdomain interactions with the F3 modules in the protein (Williams *et al*., 1982; Homandberg and Erickson, 1986; Rocco *et al*., 1987; Ingham *et al*., 1988; Khan *et al*., 1990). Of particular interest is the potential contact between the ^{1}F1^{2}F1^{3}F1^{4}F1^{5}F1 and ^{1}F3 fragments (Figure 1A), an intramolecular interaction that is believed to suppress fibronectin fibrillogenesis (Aguirre *et al*., 1994; Schwarzbauer and Sechler, 1999). While this contact would be unlikely to take place if the gelatin-binding domain had a more extended organization, akin to those of the cell-binding and heparin-binding fragments (Figure 6), the hairpin conformation of ^{6}F1^{1}F2^{2}F2 in the gelatin-binding domain may facilitate intramolecular contact between the flanking ^{1}F1^{2}F1^{3}F1^{4}F1^{5}F1 and ^{1}F3 fragments. Interestingly, the addition of collagen or the cyanogen bromide fragment CB7 of the α1(I) chain results in a reorganization and increased accumulation of fibronectin fibrils at the surface of collagen-deficient MOV-13 cells (Dzamba *et al*., 1993). Thus, collagen binding may induce a conformational change that disengages the inhibitory ^{1}F1^{2}F1^{3}F1^{4}F1^{5}F1–^{1}F3 intramolecular interaction, thus facilitating matrix assembly; this is also supported by the observed partial unfolding of plasma fibronectin upon binding of the α1(I)-CB7 fragment (Williams *et al*., 1982).

It has been proposed that stretching of the fibronectin molecule by the cell might regulate matrix function by exposing new binding sites and affecting cell adhesion (Schwarzbauer and Sechler, 1999). Applied tension could extend the molecule through a breakdown of the above interdomain interactions, the local disruption of intermodule interfaces or even complete unfolding of F3 modules (Erickson, 1994; Oberhauser *et al*., 1998; Ohashi *et al*., 1999). For example, the disruption of the ^{9}F3–^{10}F3 interface due to an extension of the intermodule linker resulted in a reduction of integrin-mediated cell adhesion and intracellular signalling (Grant *et al*., 1997). Thus, it could be argued that stretching might also provide a means for actively modulating the affinity of fibronectin for collagen by disrupting the ^{6}F1–^{2}F2 intermodule interface that enhances binding. However, the buried surface area between ^{6}F1 and ^{2}F2 in the ^{6}F1^{1}F2^{2}F2 structure ensemble is on average 868 Å^2 (±48 Å^2), much greater than the 340 Å^2 buried between ^{9}F3 and ^{10}F3 (Leahy *et al*., 1996). Therefore, the smaller and more flexible ^{9}F3–^{10}F3 interface (Copié *et al*., 1998) is likely to deform more easily in response to stress, with the result that the cell retracts from the fibronectin matrix before it can apply the necessary tension to disrupt the fibronectin–collagen interaction.

Materials and methods

Preparation of recombinant fibronectin modules

Fragments of the collagen-binding domain of human fibronectin were prepared by recombinant expression from the methylotrophic yeast *Pichia pastoris*. Expression and purification of the isolated ^{1}F2 and ^{2}F2 modules and the ^{6}F1^{1}F2 and ^{1}F2^{2}F2 module pairs have been described previously (Pickford *et al*., 1997; Sticht *et al*., 1998; Bocquier *et al*., 1999; Smith *et al*., 2000). The *P.pastoris* clone expressing the ^{6}F1^{1}F2^{2}F2 triplet (corresponding to residues 274–433 of mature human fibronectin) was produced in analogous fashion to that described previously for the ^{1}F2 module (Pickford *et al*., 1997). Expression of unlabelled and uniformly ^{15}N-labelled ([*u*-^{15}N]) proteins was carried out in a 1 l fermentor (Electrolab Ltd, Tewkesbury, UK) following the detailed protocol for the ^{4}F1^{5}F1 module pair (Bright *et al*., 1999). Each fragment was purified by a combination of cation exchange chromatography on SP-Sepharose Fast Flow (Amersham Pharmacia Biotech), affinity chromatography on gelatin–Sepharose 4B (Amersham Pharmacia Biotech) and reverse phase high-performance liquid chromatography (HPLC) on a C8 column (Rainin). Prior to the last purification step, those fragments containing the ^{2}F2 module were treated with Endo H$_f$ (New England Biolabs) to trim the high mannose sugar attached to residue Asn25 back to a single *N*-acetylglucosamine (GlcNAc) (Sticht *et al*., 1998). The identity and purity of each fragment were confirmed by electrospray mass spectrometry and N-terminal sequence analysis.

Surface plasmon resonance

The collagen α1(I) chain was purified from human placental type I collagen (Sigma) by size-exclusion chromatography through Sephacryl-S400HR (Amersham Pharmacia Biotech) followed by cation exchange chromatography at 42°C on a Mono-S HR5/5 column (Amersham Pharmacia Biotech). SPR experiments were performed on a BIAcore 2000 instrument (Biacore AB, Uppsala, Sweden). Purified collagen α1(I) chains were immobilized on the dextran matrix of a CM5 sensorchip (Biacore AB) in 10 mM acetate buffer pH 4.0, and covalently bound using the amine coupling method as described in the BIAapplications handbook (Biacore AB). A control flow cell was also created by derivatizing the surface for amine coupling in the absence of protein. For comparative binding of the fibronectin fragments, a collagen α1(I) immobilization level of ~7000 resonance units (RU) was used. In order to avoid mass transport limitation, this immobilization level was reduced to ~2000 RU for the kinetic analysis of fibronectin fragment binding. The same sensorchip surface was used in each set of experiments. Binding experiments were carried out at 25°C in HBS-EP running buffer [10 mM HEPES pH 7.4, 150 mM NaCl, 3 mM EDTA, 0.005% (v/v) Surfactant P20] at a flow rate of 20 µl/min. A regeneration step of 30 s exposure to 50 mM HCl was applied after each injection to return to the baseline. To compare the binding of the fibronectin fragments, 20 µl of 300 µM samples of ^{6}F1^{1}F2^{2}F2, ^{1}F2^{2}F2, ^{6}F1^{1}F2, ^{1}F2 and ^{2}F2 were injected over immobilized collagen α1(I) chains, and the amount of protein bound to the sensorchip was monitored by the change in RU. For the kinetic analyses, triplicates of 20 µl of five dilutions (25–200 µM) of the fibronectin fragments ^{1}F2^{2}F2 and ^{6}F1^{1}F2^{2}F2 were injected over the flow cells. The sensorgram data were analysed using global fitting procedures in the BIAevaluation 3.0 program (Karlsson and Falt, 1997). The association (k_{on}) and dissociation (k_{off}) rates were evaluated by analysing appropriate components of the sensorgram curve.

NMR spectroscopy

All NMR experiments were acquired at 25°C on a spectrometer built in-house at the Oxford Centre for Molecular Sciences incorporating an Oxford Instruments magnet (750.1 MHz for ^{1}H) and a GE/Omega computer. Experiments were recorded in a phase-sensitive manner using the States/TPPI method for quadrature detection in the indirectly detected dimensions. In all heteronuclear experiments, ^{1}H–^{15}N decoupling was achieved using a GARP pulse-train with a 1.7 kHz decoupling bandwidth. Samples for amide chemical shift comparison were prepared by dissolving either [*u*-^{15}N]^{6}F1^{1}F2, [*u*-^{15}N]^{1}F2^{2}F2 or [*u*-^{15}N]^{6}F1^{1}F2^{2}F2 to a final concentration of 1.0 mM in 90% H$_2$O/10% D$_2$O containing 1 mM 1,4-dioxane, and adjusting the pH to 4.5 (meter uncorrected for deuterium). For each sample, a one-dimensional ^{1}H spectrum and a two-dimensional gradient-enhanced [^{1}H–^{15}N]-HSQC spectrum (Kay *et al*., 1992) were acquired. Samples for ^{6}F1^{1}F2^{2}F2 assignment and structure determination were prepared by dissolving [*u*-^{15}N]^{6}F1^{1}F2^{2}F2 to a final concentration of 2.0 mM in either 90% H$_2$O/10% D$_2$O or 99.9% D$_2$O, adding 1,4-dioxane to 1 mM, and adjusting the pH to 4.5. The following spectra were recorded in H$_2$O: a two-dimensional [^{1}H–^{15}N]-HMQC-J (Kay and Bax, 1990), a three-dimensional gradient-enhanced [^{1}H–^{15}N]-TOCSY-HSQC with 46 ms mixing time (Marion *et al*., 1989) and a three-dimensional gradient-enhanced [^{1}H–^{15}N]-NOESY-HSQC with 60 ms mixing time (Marion *et al*., 1989). The following spectra were recorded in D$_2$O: a two-dimensional [^{1}H–^{1}H]-DQF-COSY (Rance *et al*., 1983), a two-dimensional [^{1}H–^{1}H]-NOESY with 60 ms mixing time (Kumar *et al*., 1980) and a two-dimensional [^{1}H–^{1}H]-TOCSY with 46 ms mixing time (Davis and Bax, 1985). For measuring the ^{15}N-{^{1}H}-NOE, two experiments were recorded, either with (NOE) or without

(NONOE) ^{1}H saturation, during the recycle delay (Kay *et al*., 1989). Slowly exchanging amide protons were identified by lyophilizing [*u*-^{15}N]$^{6}F1^{1}F2^{2}F2$ from H_2O, dissolving in D_2O and recording multiple gradient-enhanced [^{1}H–^{15}N]-HSQC spectra at two-hourly intervals.

Data processing and analysis

Data processing was performed using the FELIX 2.3 software package (Biosym Technologies Inc.). Homonuclear DQF-COSY, TOCSY and NOESY experiments were processed as described previously (Pickford *et al*., 1997). The three-dimensional gradient-enhanced [^{1}H–^{15}N]-TOCSY-HSQC and [^{1}H–^{15}N]-NOESY-HSQC data sets were processed using a Lorentzian–Gaussian multiplication in t_3, linear prediction and apodization in t_2 using a 70° phase-shifted squared sine-bell window function, and a Kaiser function for apodization in t_1. Proton chemical shifts were referenced relative to the internal standard 1,4-dioxane at 3.743 p.p.m., with indirect referencing in the ^{15}N dimension using a $^{15}N/^{1}H$ frequency ratio of 0.101329118 (Wishart *et al*., 1995). The program NMRView v3.0.b1 (Merck and Co., Inc.) was used for spectral assignment and the derivation of structural restraints. Complete assignment of the backbone N^H, H^N and Hα resonances, and of most side chain proton and nitrogen resonances of $^{6}F1^{1}F2^{2}F2$ at 25°C and pH 4.5 was achieved using standard homonuclear and heteronuclear techniques. The assignment process was assisted by previous studies on the $^{6}F1^{1}F2$ module pair (Bocquier *et al*., 1999) and the isolated $^{2}F2$ module (Sticht *et al*., 1998) under the same conditions. Backbone N^H and H^N resonances of the $^{1}F2^{2}F2$ module pair, which had previously been assigned at pH 6.0 (Smith *et al*., 2000), were reassigned at pH 4.5. An iterative procedure was used in the assignment of NOEs: those that could not be assigned unambiguously were included as ambiguous restraints during initial structure calculations (Nilges, 1995) followed, where possible, by resolution of the ambiguity by inspection of preliminary structures. NOEs were calibrated using interproton distances in regions of regular secondary structure, and converted into three distance restraint categories ('strong', 'medium' and 'weak') with upper distance limits of 2.8, 3.5 and 5.0 Å, respectively. Hydrogen bond restraints were introduced in the final round of the calculation if three criteria were met: slow solvent exchange of the H^N proton, an H^N–O distance <2.3 Å and an O–H^N–N^H angle >120° in at least 70% of the unrestrained structures. For each hydrogen bond, two distance restraints were introduced into the calculation (d_{H^N-O} = 1.7–2.3 Å and d_{N-O} = 2.4–3.3 Å). Backbone φ torsion angle restraints were derived by measuring $^{3}J_{H^N-H}\alpha$ spin–spin coupling constants from the [^{1}H–^{15}N]-HMQC-J spectra using spectral simulations (Redfield *et al*., 1991). For those residues with $^{3}J_{H^N-H}\alpha$ <6 Hz or $^{3}J_{H^N-H}\alpha$ >8 Hz, estimates of φ angles were obtained using a modified Karplus equation (Pardi *et al*., 1984) and included as restraints in the structure calculations with an error of ±30°.

Structure calculations and analysis

Structure calculations were performed using an *ab initio* simulated annealing protocol within the program CNS v0.9 (Brünger *et al*., 1998). The 'parallhdg.pro' forcefield (version 5.1) was used to describe the covalent and non-bonded interactions for the polypeptide (Linge and Nilges, 1999). Parameters for the N-linked GlcNAc on Asn25 of the $^{2}F2$ module were derived as previously described (Sticht *et al*., 1998). The non-bonded energy was calculated using a purely repulsive function with a final value of the van der Waals radii scaled by a factor of 0.75 (Linge and Nilges, 1999). A total of 100 structures were calculated using a simulated annealing profile similar to that described previously (Sticht *et al*., 1998). It comprised four stages: a high temperature conformational search phase in cartesian space (50 ps at 2000 K with a 2 fs time step), two cooling phases (2000 to 1000 K in 25 ps, and 1000 to 100 K in 25 ps, each with a 1 fs time step) and a final minimization phase. The final values for the force constants were K_{bond} = 1000 kcal/mol/Å^2, K_{angl} = 500 kcal/mol/rad^2, K_{impr} = 500 kcal/mol/rad^2, K_{vdw} = 4 kcal/mol, K_{noe} = 50 kcal/mol/Å^2 and K_{cdih} = 200 kcal/mol/rad^2. The structures were refined using an additional cycle of simulated annealing similar to the second cooling phase above, followed by extensive restrained energy minimization. The floating assignment of prochiral groups was achieved using a novel procedure named SOPHIE (for 'spinning of prochiral hydrogens'). Throughout the conformational search and cooling phases, the diastereospecifically unassigned groups were allowed to rotate freely about the bond connecting their pseudoatom and prochiral centre. Then, during the final minimization phase, each group was eased into either the pro-*R* or pro-*S* position by enforcing the correct bond angles at the prochiral centre. The stereochemical quality of the structures was assessed using the program PROCHECK_NMR (Laskowski *et al*., 1993). Buried surface areas were calculated in CNS using a probe radius of 1.4 Å. Atomic r.m.s. deviations were calculated following best-fit superposition of each accepted structure onto the secondary structure backbone heavy atoms of the lowest energy structure. The average structure was calculated by superimposing over the backbone heavy atoms (N, Cα, C) of the secondary structure elements of each module. Geometric strain was removed from this average structure by extensive restrained energy minimization in CNS (Brünger *et al*., 1998). Molecular models were generated with the programs MOLMOL (Koradi *et al*., 1996) and POV-Ray (http://www.povray.org).

Accession codes

The list of ^{1}H and ^{15}N resonance assignments of $^{6}F1^{1}F2^{2}F2$ at pH 4.5 and 25°C has been deposited at the BioMagResBank with the accession number 4830. The coordinates of the $^{6}F1^{1}F2^{2}F2$ NMR structure ensemble and the minimized average structure have been deposited in the Brookhaven Protein Data Bank with the ID codes 1e88 and 1e8b, respectively.

Acknowledgements

We thank Tony Willis, Robin Aplin, Nick Soffe and Jörn Werner for help and advice concerning N-terminal sequence analysis, electrospray mass spectrometry, NMR spectroscopy and protein dynamics. This is a contribution from the Oxford Centre for Molecular Sciences, which is supported by the BBSRC, EPSRC and MRC. A.R.P. and D.S. thank the Wellcome Trust for financial support. S.P.S. is a recipient of a Burroughs Wellcome Fund Hitchings–Elion Fellowship.

References

Aguirre,K.M., McCormick,R.J. and Schwarzbauer,J.E. (1994) Fibronectin self-association is mediated by complementary sites within the amino-terminal one-third of the molecule. *J. Biol. Chem.*, **269**, 27863–27868.

Allan,J.A., Docherty,A.J.P., Barker,P.J., Huskisson,N.S., Reynolds,J.J. and Murphy,G. (1995) Binding of gelatinases A and B to type-I collagen and other matrix components. *Biochem. J.*, **309**, 299–306.

Banyai,L. and Patthy,L. (1991) Evidence for the involvement of type II domains in collagen binding by 72 kDa type IV procollagenase. *FEBS Lett.*, **282**, 23–25.

Banyai,L., Trexler,M., Koncz,S., Gyenes,M., Sipos,G. and Patthy,L. (1990) The collagen-binding site of type-II units of bovine seminal fluid protein PDC-109 and fibronectin. *Eur. J. Biochem.*, **193**, 801–806.

Banyai,L., Tordai,H. and Patthy,L. (1994) The gelatin-binding site of human type IV collagenase (gelatinase A). *Biochem. J.*, **298**, 403–407.

Baron,M., Norman,D.G., Willis,A. and Campbell,I.D. (1990) Structure of the fibronectin type 1 module. *Nature*, **345**, 642–646.

Bocquier,A.A., Potts,J.R., Pickford,A.R. and Campbell,I.D. (1999) Solution structure of a pair of modules from the gelatin-binding domain of fibronectin. *Structure*, **7**, 1451–1460.

Bork,P., Downing,A.K., Kieffer,B. and Campbell,I.D. (1996) Structure and distribution of modules in extracellular proteins. *Q. Rev. Biophys.*, **29**, 119–167.

Bright,J.R., Pickford,A.R., Potts,J.R. and Campbell,I.D. (1999) Preparation of isotopically labelled recombinant fragments of fibronectin for functional and structural study by heteronuclear magnetic resonance spectroscopy. *Methods Mol. Biol.*, **139**, 59–69.

Briknarová,K., Grishaev,A., Banyai,L., Tordai,H., Patthy,L. and Llinas,M. (1999) The second type II module from human matrix metalloproteinase 2: structure, function and dynamics. *Structure*, **7**, 1235–1245.

Brünger,A.T. *et al*. (1998) Crystallography and NMR system (version 0.9): a new software suite for macromolecular structure determination. *Acta Crystallogr. D*, **54**, 905–921.

Campbell,I.D. and Downing,A.K. (1998) NMR of modular proteins. *Nature Struct. Biol. NMR Suppl.*, 496–499.

Collier,I.E. *et al*. (1988) H-ras oncogene-transformed human bronchial epithelial cells (TBE-1) secrete a single metalloproteinase capable of degrading basement membrane collagen. *J. Biol. Chem.*, **263**, 6579–6587.

Collier,I.E., Krasnov,P.A., Strongin,A.Y., Birkedal-Hansen,H. and Goldberg,G.I. (1992) Alanine scanning mutagenesis and functional

analysis of the fibronectin-like collagen-binding domain from human 92 kDa type IV collagenase. *J. Biol. Chem.*, **267**, 6776–6781.

Copié,V., Tomita,Y., Akiyama,S.K., Aota,S.-I., Yamada,K.M., Venable,R.M., Pastor,R.W., Krueger,S. and Torchia,D.A. (1998) Solution structure and dynamics of linked cell attachment modules of mouse fibronectin containing the RGD and synergy regions: comparison with the human fibronectin crystal structure. *J. Mol. Biol.*, **277**, 663–682.

Davis,D.G. and Bax,A. (1985) Assignment of complex ^{1}H NMR spectra via two-dimensional homonuclear Hartmann–Hahn spectroscopy. *J. Am. Chem. Soc.*, **107**, 2820–2821.

Dzamba,B.J., Wu,H., Jaenisch,R. and Peters,D.M. (1993) Fibronectin binding site in type I collagen regulates fibronectin fibril formation. *J. Cell Biol.*, **121**, 1165–1172.

Engel,J., Odermatt,E., Engel,A., Madri,J.A., Furthmayr,H., Rohde,H. and Timpl,R. (1981) Shapes, domain organizations and flexibility of laminin and fibronectin, two multifunctional proteins of the extracellular matrix. *J. Mol. Biol.*, **150**, 97–120.

Erickson,H.P. (1994) Reversible unfolding of fibronectin type III and immunoglobulin domains provides the structural basis for stretch and elasticity of titin and fibronectin. *Proc. Natl Acad. Sci. USA*, **91**, 10114–10118.

Erickson,H.P. and Carrell,N.A. (1983) Fibronectin in extended and compact conformations. Electron microscopy and sedimentation analysis. *J. Biol. Chem.*, **258**, 14539–14544.

Erickson,H.P., Carrell,N. and McDonagh,J. (1981) Fibronectin molecule visualized in electron microscopy: a long, thin, flexible strand. *J. Cell Biol.*, **91**, 673–678.

Grant,R.P., Spitzfaden,C., Altroff,H., Campbell,I.D. and Mardon,H.J. (1997) Structural requirements for biological activity of the ninth and tenth FIII domains of human fibronectin. *J. Biol. Chem.*, **272**, 6159–6166.

Hashimoto,Y., Smith,S.P., Pickford,A.R., Bocquier,A.A., Campbell,I.D. and Werner,J.M. (2000) The relative orientation of the fibronectin ^{6}F1^{1}F2 module pair: a ^{15}N NMR relaxation study. *J. Biomol. NMR*, **17**, 203–214.

Homandberg,G.A. and Erickson,J.W. (1986) Model of fibronectin tertiary structure based on studies of interactions between fragments. *Biochemistry*, **25**, 6917–6925.

Hynes,R.O. (1990) *Fibronectins*. Springer-Verlag, Berlin, Germany.

Ingham,K.C., Brew,S.A. and Isaacs,B.S. (1988) Interaction of fibronectin and its gelatin-binding domains with fluorescent labelled chains of type I collagen. *J. Biol. Chem.*, **263**, 4624–4628.

Ingham,K.C., Brew,S.A. and Migliorini,M.M. (1989) Further localization of the gelatin-binding determinants within fibronectin. *J. Biol. Chem.*, **264**, 16977–16980.

Johnson,K.J., Sage,H., Briscoe,G. and Erickson,H.P. (1999) The compact conformation of fibronectin is determined by intramolecular ionic interactions. *J. Biol. Chem.*, **274**, 15473–15479.

Karlsson,R. and Falt,A. (1997) Experimental design for kinetic analysis of protein–protein interactions with surface plasmon resonance biosensors. *J. Immunol. Methods*, **200**, 121–133.

Kay,L.E. and Bax,A. (1990) New methods for the measurement of NH–CαH coupling constants in ^{15}N-labelled proteins. *J. Magn. Reson.*, **86**, 110–126.

Kay,L.E., Torchia,D.A. and Bax,A. (1989) Backbone dynamics as studied by ^{15}N inverse detected heteronuclear NMR spectroscopy: application to staphylococcal nuclease. *Biochemistry*, **33**, 5984–6003.

Kay,L.E., Kiefer,R. and Saarinen,T. (1992) Pure absorption gradient-enhanced heteronuclear single quantum correlation spectroscopy with improved sensitivity. *J. Am. Chem. Soc.*, **114**, 10663–10665.

Khan,M.Y., Medow,M.S. and Newman,S.A. (1990) Unfolding of fibronectin and its domains. *Biochem. J.*, **270**, 33–38.

Koradi,R., Billeter,M. and Wüthrich,K. (1996) MOLMOL: a program for display and analysis of macromolecular structures. *J. Mol. Graph.*, **14**, 51–55.

Kumar,A., Ernst,R.R. and Wüthrich,K. (1980) A two-dimensional nuclear Overhauser enhancement (2D NOE) experiment for elucidation of complete proton–proton cross-relaxation networks in biological macromolecules. *Biochem. Biophys. Res. Commun.*, **95**, 1–6.

Lai,C.S., Wolff,C.E., Novello,D., Griffone,L., Cuniberti,C., Molina,F. and Rocco,M. (1993) Solution structure of human plasma fibronectin under different solvent conditions: fluorescence energy transfer, circular dichroism and light-scattering studies. *J. Mol. Biol.*, **230**, 625–640.

Laskowski,R.A., MacArthur,M.W., Moss,D.S. and Thornton,J.M. (1993) PROCHECK: a program to check the stereochemical quality of protein structures. *J. Appl. Crystallogr.*, **24**, 946–950.

Leahy,D.J., Aukhil,I. and Erickson,H.P. (1996) 2.0 Å crystal structure of a four-domain segment of human fibronectin encompassing the RGD loop and synergy region. *Cell*, **84**, 155–164.

Linge,J.P. and Nilges,M. (1999) Influence of non-bonded parameters on the quality of NMR structures: a new force field for NMR structure calculation. *J. Biomol. NMR*, **13**, 51–59.

Litvinovich,S.V., Strickland,D.K., Medved,L.V. and Ingham,K.C. (1991) Domain structure and interactions of the type I and type II modules in the gelatin-binding region of fibronectin. All six modules are independently folded. *J. Mol. Biol.*, **217**, 563–575.

Marion,D., Driscoll,P.C., Kay,L.E., Wingfield,P.T., Bax,A., Gronenborn, A.M. and Clore,G.M. (1989) Overcoming the overlap problem in the assignment of ^{1}H-NMR spectra of larger proteins by use of 3-dimensional ^{1}H–^{15}N Hartman Hahn multiple quantum coherence and nuclear Overhauser multiple quantum coherence spectroscopy. *Biochemistry*, **28**, 6150–6156.

Morgunova,E., Tuuttila,A., Bergmann,U., Isupov,M., Lindqvist,Y., Schneider,G. and Tryggvason,K. (1999) Structure of human pro-matrix metalloproteinase-2: activation mechanism revealed. *Science*, **284**, 1667–1670.

Murphy,G., Nguyen,Q., Cockett,M.I., Atkinson,S.J., Allan,J.A., Knight, C.G., Willenbrock,F. and Docherty,A.J. (1994) Assessment of the role of the fibronectin-like domain of gelatinase A by analysis of a deletion mutant. *J. Biol. Chem.*, **269**, 6632–6636.

Nilges,M. (1995) Calculation of protein structures with ambiguous distance restraints: automated assignment of ambiguous NOE crosspeaks and disulphide connectivities. *J. Mol. Biol.*, **245**, 645–660.

Oberhauser,A.F., Marszalek,P.E., Erickson,H.P. and Fernandez,J.M. (1998) The molecular elasticity of the extracellular matrix protein tenascin. *Nature*, **393**, 181–185.

Ohashi,T., Kiehart,D.P. and Erickson,H.P. (1999) Dynamics and elasticity of the fibronectin matrix in living cell culture visualized by fibronectin–green fluorescent protein. *Proc. Natl Acad. Sci. USA*, **96**, 2153–2158.

Owens,R.J. and Baralle,F.E. (1986) Mapping the collagen-binding site of human fibronectin by expression in *Escherichia coli*. *EMBO J.*, **5**, 2825–2830.

Pardi,A., Billeter,M. and Wüthrich,K. (1984) Angular dependence of the amide proton–Cα proton coupling constants, $^{3}J_{HN}\alpha$, in a globular protein. *J. Mol. Biol.*, **180**, 741–751.

Pickford,A.R., Potts,J.R., Bright,J.R., Phan,I. and Campbell,I.D. (1997) Solution structure of a type 2 module from fibronectin: implications for the structure and function of the gelatin-binding domain. *Structure*, **5**, 359–370.

Rance,M., Sørensen,O.W., Bodenhausen,G., Wagner,G., Ernst,R.R. and Wüthrich,K. (1983) Improved spectral resolution in COSY ^{1}H NMR spectra of proteins via double quantum filtering. *Biochem. Biophys. Res. Commun.*, **177**, 479–485.

Redfield,C., Smith,L.J., Boyd,J., Lawrence,G.M., Edwards,R.G., Smith,R.A. and Dobson,C.M. (1991) Secondary structure and topology of human interleukin 4 in solution. *Biochemistry*, **30**, 11029–11035.

Rocco,M., Carson,M., Hantgan,R., McDonagh,J. and Hermans,J. (1983) Dependence of the shape of the plasma fibronectin molecule on solvent composition. Ionic strength and glycerol content. *J. Biol. Chem.*, **258**, 14545–14549.

Rocco,M., Infusini,E., Daga,M.G., Gogioso,L. and Cuniberti,C. (1987) Models of fibronectin. *EMBO J.*, **6**, 2343–2349.

Schwarzbauer,J.E. and Sechler,J.L. (1999) Fibronectin fibrillogenesis: a paradigm for extracellular matrix assembly. *Curr. Opin. Cell Biol.*, **11**, 622–627.

Sharma,A., Askari,J.A., Humphries,M.J., Jones,E.Y. and Stuart,D.I. (1999) Crystal structure of a heparin- and integrin-binding segment of human fibronectin. *EMBO J.*, **18**, 1468–1479.

Sicheri,F., Moarefi,I. and Kuriyan,J. (1997) Crystal structure of the Src family tyrosine kinase Hck. *Nature*, **385**, 602–609.

Skorstengaard,K., Holtet,T.L., Etzerodt,M. and Thorgersen,H.C. (1994) Collagen-binding recombinant fibronectin fragments containing type II domains. *FEBS Lett.*, **343**, 47–50.

Smith,S.P., Hashimoto,Y., Pickford,A.R., Campbell,I.D. and Werner,J.M. (2000) Interface characterization of the type II module pair from fibronectin. *Biochemistry*, **39**, 8374–8381.

Steffensen,B.J., Wallon,U.M. and Overall,C.M. (1995) Extracellular matrix binding properties of recombinant fibronectin type II-like modules of human 72-kDa gelatinase/type IV collagenase. High

affinity binding to native type I collagen but not native type IV collagen. *J. Biol. Chem.*, **270**, 11555–11566.

Sticht,H., Pickford,A.R., Potts,J.R. and Campbell,I.D. (1998) Solution structure of the glycosylated second type 2 module of fibronectin. *J. Mol. Biol.*, **276**, 177–187.

Wilhelm,S.M., Collier,I.E., Marmer,B.L., Eisen,A.Z., Grant,G.A. and Goldberg,G.I. (1989) SV40-transformed human lung fibroblasts secrete a 92 kDa type IV collagenase which is identical to that secreted by normal human macrophages. *J. Biol. Chem.*, **264**, 17213–17221.

Williams,E.C., Janmey,P.A., Ferry,J.D. and Mosher,D.F. (1982) Conformational states of fibronectin. *J. Biol. Chem.*, **257**, 14973–14978.

Wishart,D.S., Bigam,C.G., Yao,J., Abildgaard,F., Dyson,H.J., Oldfield,E., Markley,J.L. and Sykes,B.D. (1995) ^{1}H, ^{13}C and ^{15}N chemical shift referencing in biomolecular NMR. *J. Biomol. NMR*, **6**, 135–140.

Received November 29, 2000; revised January 23, 2001; accepted February 2, 2001